Inorganic Chemistry

Article

pubs.acs.org/IC

Theory of Divalent Main Group H_2 Activation: Electronics and Quasiclassical Trajectories

Deepa Devarajan,[†] Charles E. Doubleday,*[,‡] and Daniel H. Ess*[,†]

[†]Department of Chemistry and Biochemistry, Brigham Young University, Provo, Utah 84602, United States

[‡]Department of Chemistry, Columbia University, New York 10027, United States

Supporting Information

ABSTRACT: Density functional theory (DFT), absolutely localized molecular orbital (ALMO) analysis, and quasiclassical trajectories (QCTs) were used to study the structure, barrier heights, thermodynamics, electronic properties, and dynamics of dihydrogen (H_2) activation by singlet divalent main group compounds (ER_2; E = C, Si, Ge). ALMO energy and charge decomposition calculations reveal that in the transition state CR_2 acts as an ambiphile toward H_2 because of equal forward-bonding and back-bonding orbital stabilization while SiR_2 and GeR_2 act as nucleophiles with dominant orbital energy stabilization arising from ER_2 to H_2 donation. Frontier molecular orbital (FMO) energy gaps do not provide a reasonable estimate of energy stabilization gained between the ER_2 and H_2 in the transition state or an accurate description of the nucleophilic versus electrophilic character because of electron repulsion and orbital overlap influences that are neglected. In CR_2 transition states, forward-bonding and back-bonding are maximized in the nonleast motion geometry. In contrast, SiR_2/GeR_2 transition states have side-on geometries to avoid electron−electron repulsion. Electron repulsion, rather than orbital interactions, also determines the relative barrier heights of CR_2 versus SiR_2/GeR_2 reactions. Examination of barrier heights and reaction energies shows a clear kinetic-thermodynamic relationship for ER_2 activation of H_2. A computational survey of R groups on ER_2 divalent atom centers was performed to explore the possibility for H_2 activation to occur with a low barrier and thermodynamically reversible. QCTs show that dihydrogen approach and reaction with CR_2 may involve geometries significantly different than the static transition-state structure. In contrast, trajectories for dihydrogen addition to SiR_2 involve geometries close to the side-on approach suggested by the static transition-state structure. QCTs also demonstrate that addition of H_2 to CR_2 and SiR_2 is dynamically concerted with the average time gap of bond formation between E−H bonds of approximately 11 and 21 fs, respectively.

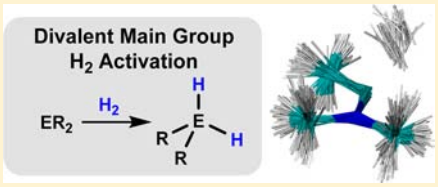

INTRODUCTION

Transition metal−ligand complexes have generally provided a successful platform for homogeneous dihydrogen (H_2) activation reactions.[1] However, there is now an emerging alternative strategy for H_2 activation based on using main group compounds.[2,3] This strategy entails H_2 bond cleavage by either a single main group atom center from a divalent compound (ER_2, E = C, Si, Ge), which has been analogized to transition metal-mediated oxidative addition, or by heterolytic cleavage of H_2 promoted by multiatom centers comprising a Lewis acid−base complex (Scheme 1).[4−8]

Power and co-workers reported the first well-defined example of H_2 activation by a heavy main group compound using digermyne (Ar′GeGeAr′) (Ar′ = C_6H_3-2,6(C_6H_3-2,6-Pr^i_2)$_2$).[3e] In this report Power speculated that H_2 activation results from the interaction between the H_2 highest occupied molecular orbital (HOMO) and the digermyne lowest unoccupied molecular orbital (LUMO). Power also showed that distannyne (Ar′SnSnAr′) and low-valent Group 13 metal complexes (GaAr′) were also competent to induce H_2 activation.[3h,i] More recently, Jones, Frenking, and co-workers showed that digermyne (LGeGeL) [L = N(SiMe$_3$)Ar*; Ar* = 4-Me-2,6-{C(H)-Ph$_2$}$_2$C$_6$H$_2$] also activates dihydrogen in solution or solid state.[3j]

Scheme 1. Comparison of Dihydrogen Activation Strategies

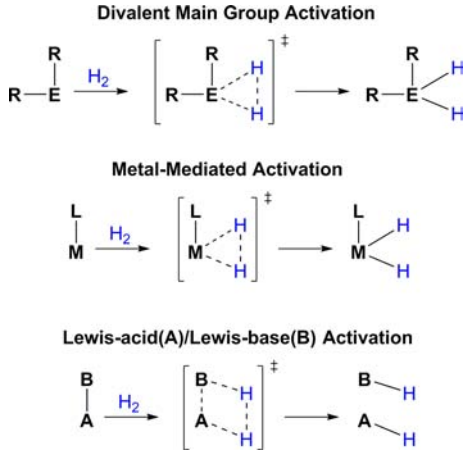

Most germane to our current work, Bertrand and co-workers reported that divalent (alkyl)(amino)carbenes readily activate H_2 under mild conditions (Scheme 2).[4c] In contrast, di(amino)-

Received: April 25, 2013
Published: July 9, 2013

   dx.doi.org/10.1021/ic4010399 | Inorg. Chem. 2013, 52, 8820−8833

Scheme 2. Examples of (Alkyl)(Amino)Carbene Activation of Dihydrogen Reported by Bertrand[4c]

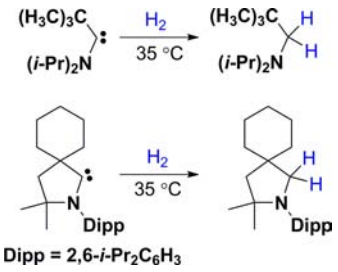

carbenes are unreactive.[4c] Importantly, (alkyl)(amino)carbene activation of H_2 is highly exothermic and irreversible. This reactivity is reminiscent of early σ bond activation chemistry reported by Bergman[9] using the $(Cp^*)(PR_3)Ir$ complex, which via the frontier orbital isolobal analogy have been compared to divalent main group compounds.[10] On the basis of frontier orbital energies and atomic charges, Bertrand proposed that (alkyl)(amino)carbenes behave as nucleophiles toward H_2. The nucleophilic activation of H_2 by divalent carbon can also be contrasted with the conventional view that transition metal complexes are Lewis acidic.[11] However, our group previously showed that transition metal−ligand complexes can act as either electrophiles or nucleophiles toward H_2 during bond activation.[12]

Jones, Mountford, Aldrige, and co-workers recently reported that the acyclic silylene $Si\{B(NDippCH)_2\}\{N\text{-}(SiMe_3)Dipp\}$ (Dipp = 2,6-*i*pr$_2$C$_6$H$_3$) also activates H_2 in a concerted route.[4d] However, silylene and carbene transition-structure geometries are significantly different (Scheme 3). In the silylene transition

Scheme 3. Possible Trajectories of H_2 Approach to Divalent Main Group Compounds (ER_2) during Activation

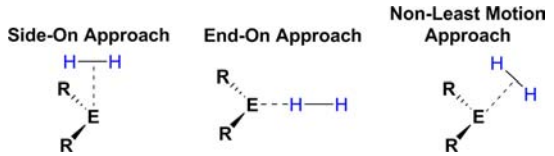

structure H_2 approaches from a side-on trajectory while in the carbene transition structure H_2 approaches from what has been termed the "non-least motion" trajectory.[13] Jones and co-workers also speculated that silylene acts as an electrophilic partner to activate H_2 with characteristics more like a transition metal than a carbene. However, this is contrary to the expectation that Si is more electropositive than carbon.

Our group recently presented a general classification and understanding of electronic properties of dihydrogen and carbon−hydrogen bond activation transition states mediated by transition metal−ligand complexes.[12,14] Our studies revealed that in activation reactions transition metals can act as either electrophilic, ambiphilic, or nucleophilic partners toward σ bonds, and this characteristic can be understood based on the direction of net charge transfer energy stabilization resulting from forward-bonding and back-bonding orbital interactions (Scheme 4). It was also shown that the extent to which the H_2 bond is activated in the transition-structure geometry depends on back-bonding orbital interactions and not forward-bonding orbital interactions, regardless of the mechanism or overall charge flow.

Scheme 4. Illustration of Forward-Bonding and Back-Bonding Frontier Orbital Interactions in Metal-Mediated Dihydrogen Activation

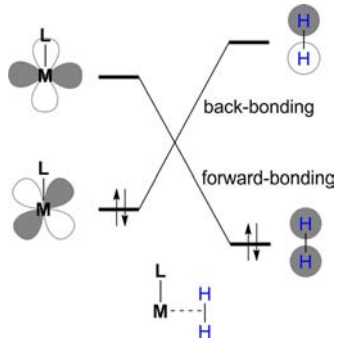

Here we present a comprehensive static and dynamical view of H_2 activation by singlet divalent main group compounds (Scheme 5) using density functional theory (DFT), absolutely

Scheme 5. Experimentally Known and Model Divalent Main Group Compounds Analyzed for H_2 Activation

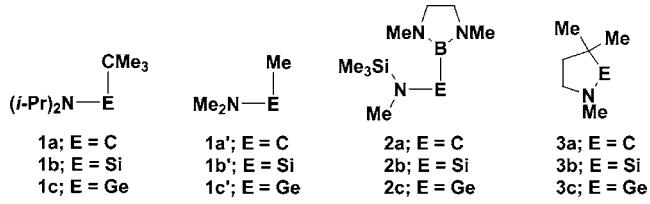

localized molecular orbital (ALMO) analysis, and quasiclassical trajectories (QCTs). This analysis provides insight into the origin of the activation barriers, transition-state geometries, and reaction pathways for ER_2 (E = C, Si, Ge) H_2 activation. QCTs provide additional insight into the dynamical motion of side-on versus the nonleast motion approaches of dihydrogen and timing of E−H bond formation and H−H bond cleavage during activation. This work also examines barrier heights and thermodynamics for concerted H_2 activation by group 14 compounds with a variety of R groups to probe whether kinetically fast and thermodynamically reversible H_2 activation is possible. Lastly, in conjunction with our previous work, this study provides a comparison of main group-mediated versus transition metal-mediated H_2 activation reactions.

THEORY AND COMPUTATIONAL DETAILS

All geometries were optimized in Gaussian 03 or 09[15] using (U)B3LYP/6-31G(d,p) DFT. Stationary points were characterized as minima or first-order saddle points by vibrational frequency analysis from the Hessian matrix. All (U)CCSD(T) energies were computed in Gaussian 09. Absolutely localized molecular orbital (ALMO) energy and charge decomposition analyses were carried out using Q-Chem 3.2.[16,17] Scheme 6a defines the transition structure fragments (ER_2 and H_2) and direction of charge transfer used in the ALMO energy and charge analysis.

The ALMO energy and charge analysis utilizes block localization of fragment molecular orbital coefficients to obtain directional electron charge transfer (ΔQ) and energy stabilization (E_{CT}) that results from the difference between localized and delocalized electronic states. This provides a means to quantitatively evaluate chemically intuitive donor−acceptor orbital interactions. This method is advantageous because it variationally optimizes the localized intermediate DFT wave function and the strong fragment localization results in small basis set effects. Orbital charge transfer energy stabilization is only part of the total

dx.doi.org/10.1021/ic4010399 | Inorg. Chem. 2013, 52, 8820−8833

Scheme 6. (a) Definition of Transition-State Fragments Used for Energy and Charge Decomposition Analysis, and (b) Qualitative Potential Energy Diagram Depicting Distortion, Interaction, and Activation Energies

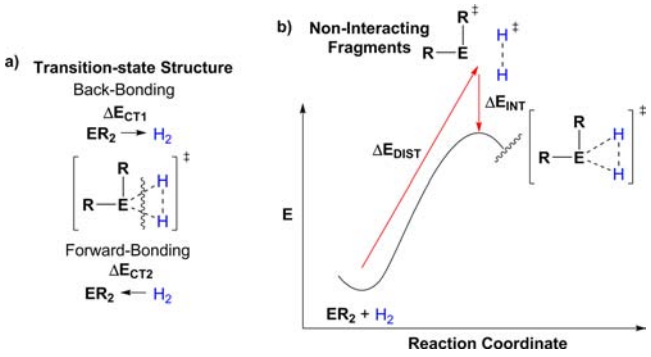

transition state interaction energy between reacting ER_2 and H_2 fragments. Equations 1 and 2 define the total transition-state activation energy and the interaction energy components. The ΔE_{DIST} energy term is the energy to distort the ER_2 and H_2 fragments from their ground-state structure into their respective transition-state geometries (Scheme 6b). The interaction energy (ΔE_{INT}) mitigates/controls the energy penalty for geometric distortion and is divided into three terms (ΔE_{FRZ}, ΔE_{POL}, and ΔE_{CT}). Dissection of interaction energy into these types of energy terms was introduced by Morokuma, Rauk and Ziegler, and others and has been pioneered and popularized by Bickelhaupt.[18] The ALMO flavor of energy decomposition analysis has been extensively used by our group.[12,14]

$$\Delta E^{\ddagger} = \Delta E_{DIST} + \Delta E_{INT} \quad (1)$$

$$\Delta E_{INT} = \Delta E_{FRZ} + \Delta E_{POL} + \Delta E_{CT} \quad (2)$$

In the ALMO analysis the three interaction energy components are obtained by bringing together the ER_2 and H_2 fragments in their transition-state geometry while enforcing absolute localization of the molecular orbitals on each fragment and an antisymmetrized wave function description to comply with the Pauli exclusion principle. This allows static (frozen) electron densities to overlap but without orbital relaxation and gives the frozen density term (ΔE_{FRZ}) that is a combination of Coulombic (electrostatic) and exchange (Pauli) repulsion. Fragment polarization (ΔE_{POL}) is then evaluated by allowing variational intramolecular relaxation of the ALMOs due to the presence of the other fragment. Lastly, an estimate of directional charge transfer (ΔE_{CT}) stabilization is obtained variationally by the difference between this localized state and the fully delocalized state. The ΔE_{CT} energy term provides an estimate of all occupied to unoccupied orbital interactions between transition-state fragments where ΔE_{CT1} is the energy stabilization due to electron flow from ER_2 to H_2 (ΔQ_1) while ΔE_{CT2} is the energy stabilization due to electron flow from H_2 to ER_2 (ΔQ_2). The total charge transfer (eq 3) also includes a small higher-order term (ΔE_{HO}). ALMO electronic energies are not zero-point corrected.

$$\Delta E_{CT} = \Delta E_{CT1} + \Delta E_{CT2} + \Delta E_{HO} \quad (3)$$

Dynamics of H_2 addition to **1a′** and **1b′** were explored by quasiclassical trajectories (QCTs) at the (U)B3LYP/6-31G(d,p) level of theory with a broken spin initial guess at each point. A customized version of Venus[19] was used to select initial coordinates and momenta by transition state (TS) normal mode sampling,[20] and trajectories were integrated by Gaussian 09 with the BOMD option. The sampling procedure randomly distorts the saddle point to generate a set of structures whose coordinates and momenta approximate a quantum mechanical Boltzmann distribution of vibrational levels on the TS dividing surface at 300 K. Trajectories were propagated in the forward and reverse directions from the initial TS point until the reactants are separated by greater than 2.5 Å or C−H bonds less than 1.09 Å and Si−H bonds less than 1.46 Å.

The choice of (U)B3LYP for energy decomposition analysis and QCTs was based on good agreement between the (U)B3LYP intrinsic reaction coordinate (IRC) energy profile with the (U)CCSD(T)/6-311G(d,p) energy profile (see Supporting Information). Also, an ab initio benchmark study showed that B3LYP performs very well for similar bond activation reactions.[21] Also, B3LYP deviates by less than 3 kcal/mol from coupled-cluster with single and double and perturbative triple excitations [CCSD(T)] for singlet−triplet gap energies of **1a′**, **1b′**, and **1c′** and activation and reaction energies for addition of H_2 (see Supporting Information).

RESULTS AND DISCUSSION

H_2 Activation Transition-Structure Geometries. To begin, Figure 1 shows the transition-structure geometries for H_2 activation by divalent compounds **1**−**3**. Divalent **1a** is the (alkyl)(amino)carbene compound reported by Bertrand that readily activates H_2 (Schemes 2).[4c] Compounds **1b** and **1c** substitute Si and Ge for the divalent carbon center. **2b** is a model acyclic silylene for Si{B(NDippCH)$_2$}{N-(SiMe$_3$)Dipp}[4d] in which the Dipp group is replaced by a methyl group. Compounds **2a** and **2c** are the analogues of **2b** in which carbon and Ge are substituted for the Si atom center. Compound **3a** is a model cyclic (alkyl)(amino)carbene similar to the experimental system reported by Bertrand (Scheme 2).[4c] Compounds **3b** and **3c** are the Si and Ge heavy atom analogues of **3a**.

The H1−H2 partial bond length in **TS1a** is 0.941 Å and increases to 1.034 Å and to 1.148 Å in **TS1b** and **TS1c**. In these transition structures the E−H1 bond lengths are significantly shorter than the E−H2 bond lengths. This suggests very asynchronously timed activation and perhaps even dynamically two-step. For example, in **TS1a** the C−H1 partial bond distance is 0.513 Å shorter than the C−H2 bond partial bond distance. However, the difference in E−H partial bond lengths is smaller when E = Si and Ge compared to E = C. In **TS1b** and **TS1c** the partial bond length differences are 0.16 and 0.19 Å. These general patterns of partial bond lengths and asynchronously timed H_2 activation are also exhibited in transition structures **TS2** and **TS3**.

Inspection of the transition-structure geometries show disparate approaches of H_2 to the E atom center, which has been pointed out previously.[4d] Scheme 7 defines θ1, θ2, and d geometrics that can be used to compare the approach of H_2 to the C, Si, and Ge atoms along the reaction coordinate and at the transition state. The distance d is from E to the center of the H1−H2 bond. θ1 defines the angle between the R-E-R plane and the plane that passes through the center of the H1−H2 bond and E. θ2 is defined as the angle between the plane that passes through the center of the H1−H2 bond and E and the molecular plane of H_2. When angles θ1 and θ2 are equal to 90° the transition-state geometry adopts what was termed as the side-on approach of H_2 (Scheme 3). When θ1 equals 180° and θ2 equals zero then the transition-state geometry adopts an end-on approach of H_2. Another possible extreme geometry occurs when θ1 equals 180° and θ2 equals 90°. The so-called nonleast-motion approach involves θ1 approximately equal to 135° and θ2 equal to 45−90°.

The distance d in **TS1** is ∼1.5 Å and does not change significantly between **TS1a**, **TS1b**, and **TS1c**. In **TS1a** θ1 = 132° and θ2 = 48°, which is typical of H_2 approach to a carbene carbon atom and is considered to be a nonleast-motion approach (Scheme 3). This is an intermediate geometry between the extremes shown in Scheme 7a and 7c. In contrast, **TS1b** and **TS1c** have θ1 and θ2 angles close to ∼115° and ∼80°, respectively. These angles support the description of these transition states as a side-on approach of H_2 to Si and Ge. This suggests that in **TS1b** and **TS1c** the H_2 approach to Si and Ge

dx.doi.org/10.1021/ic4010399 | Inorg. Chem. 2013, 52, 8820−8833

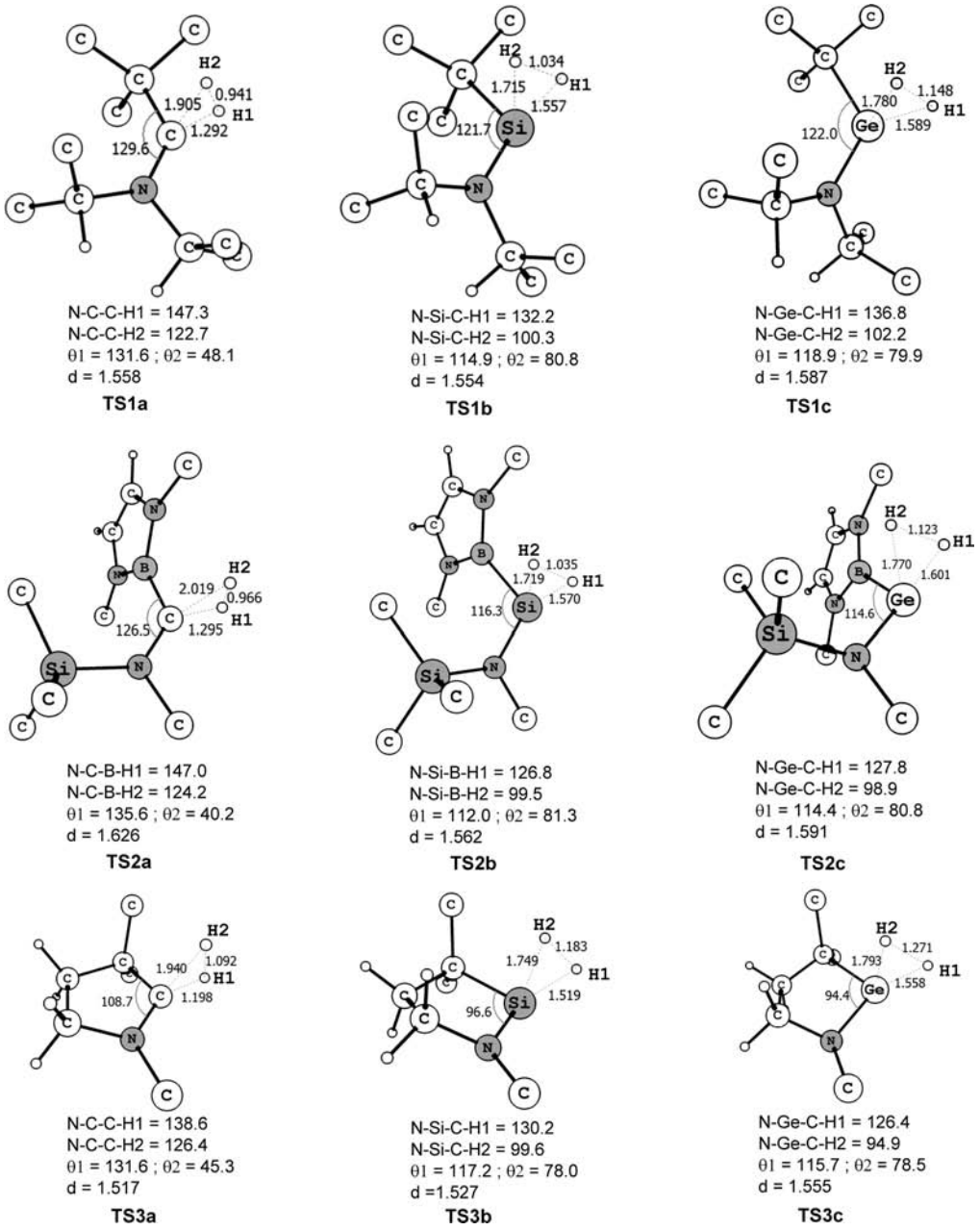

Figure 1. B3LYP/6-31G(d,p) transition-structure geometries. The hydrogen atoms on the methyl groups were removed for visual clarity. Bond lengths reported in Å and angles reported in degrees.

Scheme 7. Definition of $\theta 1$, $\theta 2$, and d for Three Different H_2 Activation Approaches

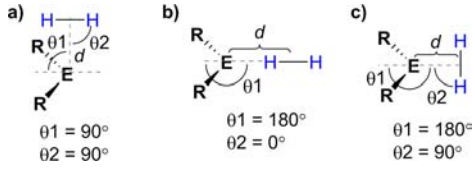

Scheme 8. Possible Frontier Orbital Interactions for ER_2-Mediated H_2 Activation

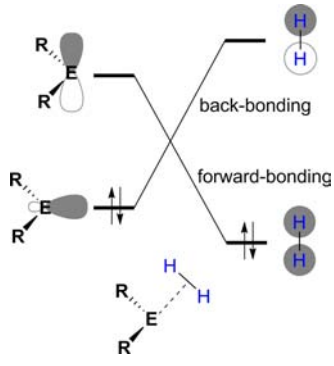

atoms may be significantly asynchronous along the reaction pathway toward the tetrahedral addition product.

In general the geometrics of **TS2** and **TS3** and the changes from E = C to Si to Ge are similar to **TS1**. Significant geometric differences between carbon compounds and heavier main-group analogues is well-known for many compounds. For example the

dx.doi.org/10.1021/ic4010399 | Inorg. Chem. 2013, 52, 8820−8833

Table 1. B3LYP/6-311G(d,p)//B3LYP/6-31G(d,p) ALMO Energy Decomposition Results[a]

	$\Delta E^{\ddagger}$	ΔE_{rxn}	ΔE_{DIST}	ΔE_{INT}	ΔE_{FRZ}	ΔE_{POL}	ΔE_{CT1}	ΔE_{CT2}	[b] ΔE_{HO}
TS1a	15.4	−66.0	16.5	−1.1	92.9	−26.5	−35.5	−29.1	−2.9
TS1b	19.1	−47.8	28.6	−9.5	112.9	−54.0	−44.6	−28.9	5.0
TS1c	32.4	−25.8	41.5	−9.1	117.1	−53.4	−45.0	−31.0	3.2
TS2a	12.9	−62.2	18.0	−5.1	90.1	−29.3	−36.8	−26.1	−3.1
TS2b	15.4	−44.3	29.4	−14.0	101.5	−47.0	−44.0	−28.5	4.0
TS2c	26.1	−25.6	41.7	−15.6	102.3	−47.5	−41.6	−30.5	1.8
TS3a	23.0	−53.5	33.8	−10.8	125.8	−45.5	−53.7	−36.1	−1.2
TS3b	37.0	−31.1	44.3	−7.2	143.0	−64.8	−70.8	−31.0	16.3
TS3c	47.6	−10.9	57.6	−10.0	134.0	−60.7	−57.6	−33.3	7.5

[a]All ALMO energy values are basis-set superposition corrected. (kcal/mol). [b]Higher-order charge transfer energy stabilization cannot be assigned to a particular direction of charge flow.

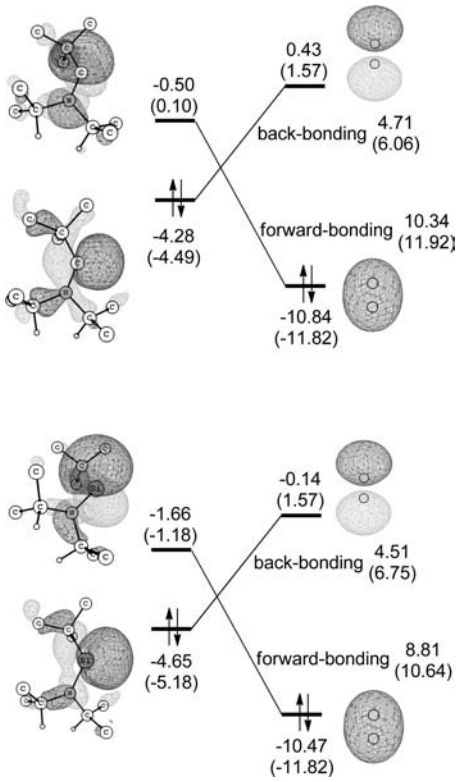

Figure 2. B3LYP/6-311G(d,p)//B3LYP/6-31G(d,p) Kohn−Sham FMO energies and intermolecular orbital energy gaps for transition-state fragments for **TS1a** (top) and **TS1b** (bottom). Values reported in parentheses are for fully optimized ground state reactants. (eV).

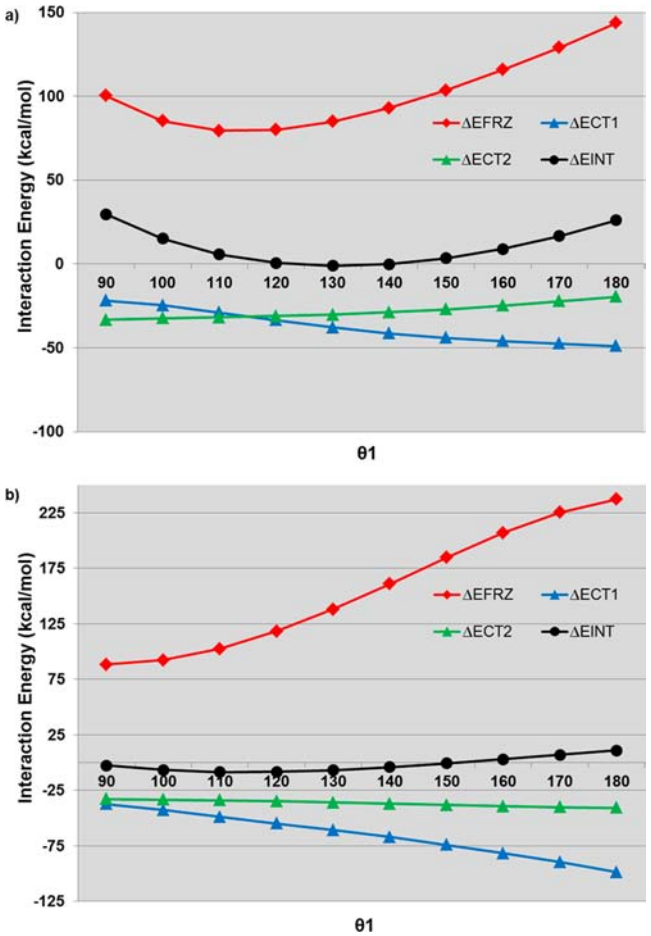

Figure 3. Plot of B3LYP/6-31G(d,p) ALMO energies for the interaction of H_2 with (a) **1a** and (b) **1b** as a function of θ1.

heavier homologues of alkene, alkyne, HCN, and HNC adopt distorted geometries.[22]

Transition Structure Energy and Charge Analysis. As discussed in the Introduction, our group has previously analyzed the bonding interactions along the reaction pathway for H_2 addition to metal−ligand complexes with a focus on forward-bonding and back-bonding orbital interactions (Scheme 4). Similarly, divalent main group ER_2 activation of H_2 is expected to have forward-bonding and back-bonding interactions depicted in Scheme 8. However, the orbital analogy is not perfect, and may in fact be problematic, because of the difference in frontier orbital symmetries of ER_2 compounds and transition metal centers. For example, in transition metal centers the occupied orbital has π symmetry while the vacant orbital has σ symmetry. In contrast, for ER_2 compounds the occupied orbital has σ symmetry while the vacant orbital has π symmetry. The frontier orbital symmetry of ER_2 compounds is often invoked in explaining a nonleast-motion pathway for addition of H_2.[13a,b]

To examine the forward-bonding and back-bonding interactions and the resulting energy stabilization that occurs for H_2 activation by ER_2 compounds **1**−**3** the ALMO energy and charge decomposition analysis was used. Results from the ALMO analysis of the transition structures are reported in Table 1. The Supporting Information shows the relative insensitivity of the ALMO energy terms with increasing basis set size.

dx.doi.org/10.1021/ic4010399 | Inorg. Chem. 2013, 52, 8820−8833

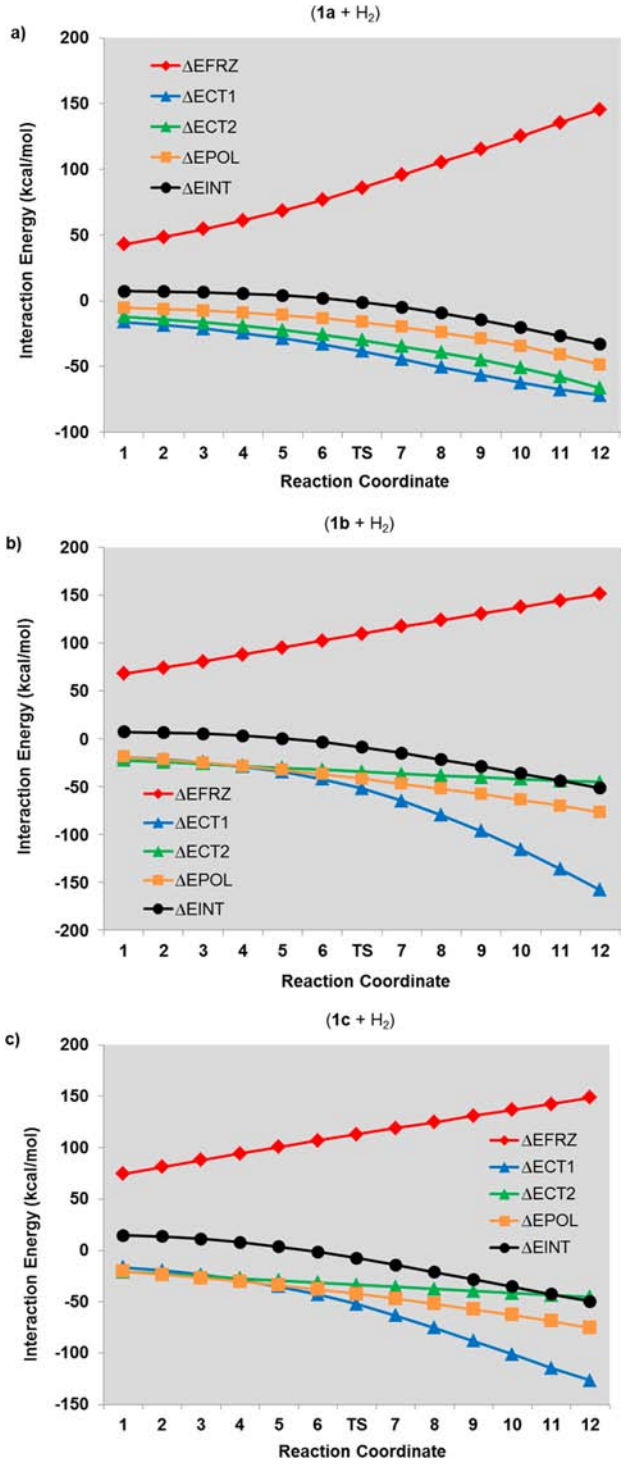

Figure 4. Plot of B3LYP/6-31G(d,p) ALMO interaction energies along 12 IRC points, including the transition state, for H_2 activation. The H–H partial bond distances along the IRC pathway ranges between (a) 0.817–1.170 Å, (b) 0.842–1.358 Å, and (c) 0.864–1.479 Å.

The activation energy ($\Delta E^{\ddagger}$) for **TS1a** is 15.4 kcal/mol and increases to 19.1 and 32.4 kcal/mol for **TS1b** and **TS1c**, respectively. In **TS1a** $\Delta E^{\ddagger}$ is dominated by geometrical distortion (ΔE_{DIST}) that requires 16.5 kcal/mol to achieve the transition-structure geometry, mainly due to H_2 stretching. This energy penalty is mitigated by only −1.1 kcal/mol of total interaction (ΔE_{INT}) between fragments. This large distortion energy and small interaction energy is in accordance with the reaction force analysis by Toro-Labbé.[23] However, this small ΔE_{INT} value is the result of large stabilizing and destabilizing interactions that are almost counterbalanced. For example, in **TS1a** there is significant closed-shell (Pauli) repulsion between ER_2 and H_2 that overwhelms electrostatic attraction to give a ΔE_{FRZ} value of 92.9 kcal/mol. This large destabilizing repulsion almost entirely mitigates the effects of intramolecular fragment orbital polarization (ΔE_{POL}) that results in −26.5 kcal/mol of stabilization and the back-bonding and forward-bonding orbital charge transfer interactions ΔE_{CT1} and ΔE_{CT2} that are stabilizing by −35.5 and −29.1 kcal/mol, respectively. Therefore, the large distortion energy in **TS1a** results from H_2 stretching to narrow its intramolecular HOMO–LUMO gap to increase polarization and intermolecular orbital interactions to overcome the significant closed-shell repulsion.

Scheme 9. Thermodynamic Cycle

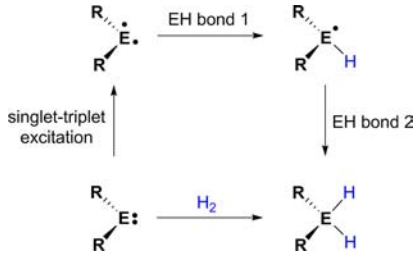

Table 2. B3LYP Activation and Reaction Energies (kcal/mol)

	E = C		E = Si		E = Ge	
compound	$\Delta E^{\ddagger}$	ΔE_{rxn}	$\Delta E^{\ddagger}$	ΔE_{rxn}	$\Delta E^{\ddagger}$	ΔE_{rxn}
$E(H)(NH_2)$	13.2	−69.8	26.1	−36.2	34.5	−22.2
$E(H)(NMe_2)$	13.8	−66.6	28.8	−33.8	36.8	−19.8
E(H)(OH)	5.4	−86.2	21.8	−44.2	31.2	−27.3
E(H)(OMe)	6.2	−84.3	23.1	−42.5	31.5	−26.7
E(H)(F)	1.4	−98.8	18.6	−49.5	28.7	−31.6
E(H)(Cl)	1.9	−106.1	17.9	−47.1	27.3	−30.6
E(H)(Ph)	2.2	−105.4	9.9	−51.6	16.6	−38.6
$E(NH_2)_2$	32.6	−43.2	43.0	−28.2	53.0	−11.8
$E(NMe_2)_2$	24.9	−50.8	42.6	−30.6	50.9	−14.0
$E(OH)_2$	32.6	−54.4	47.3	−34.1	56.8	−13.8
$E(OMe)_2$	24.2	−69.5	45.6	−34.3	56.1	−14.3
$E(CH_3)_2$	2.3	−105.6	9.8	−57.3	15.2	−44.0
$E(BH_2)_2$	7.6	−50.7	1.2	−32.7	6.3	−23.8
$E(F)_2$	29.4	−67.6	52.3	−34.4	65.3	−11.7
$E(Cl)_2$	15.4	−86.2	41.6	−33.6	54.3	−12.8

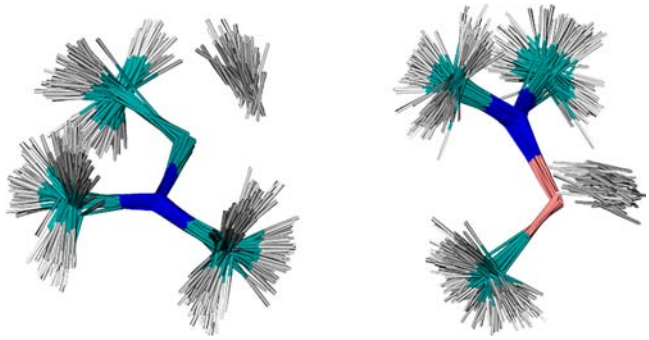

Figure 5. Overlay of geometries on the transition-state dividing surface chosen by normal mode sampling for **1a′** and H_2 (left) and **1b′** and H_2 (right).

dx.doi.org/10.1021/ic4010399 | Inorg. Chem. 2013, 52, 8820–8833

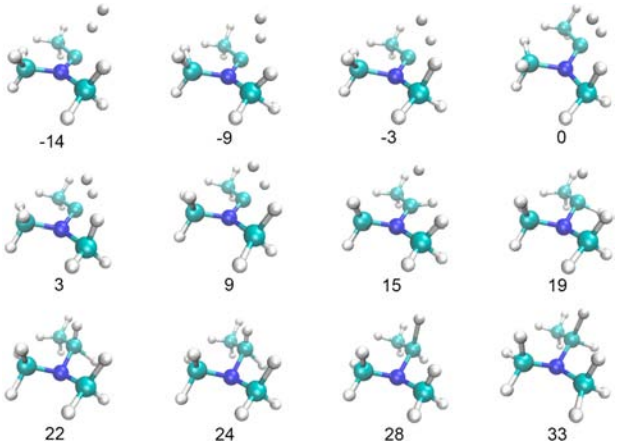

Figure 6. Plot of typical trajectory for reaction between **1a′** and H_2 with a time gap of 7 fs between the two forming C−H bonds.

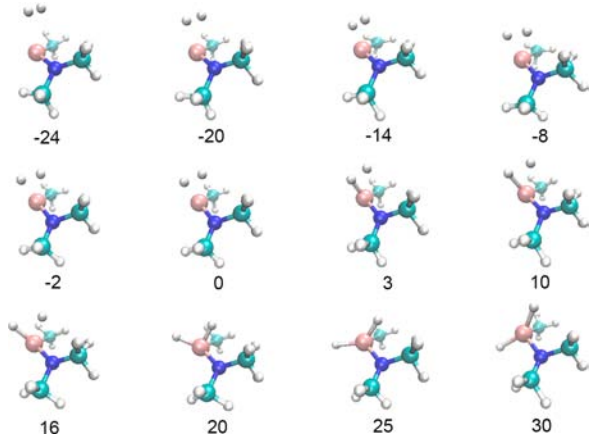

Figure 7. Plot of typical trajectory for reaction between **1b′** and H_2. (fs) Time gap between Si−H bond formation is 17 fs.

Although the ALMO ΔE_{CT} values are a sum of all occupied to unoccupied orbital interactions, it is expected that back-bonding energy stabilization results mainly from charge transfer from the HOMO hybrid-type orbital of **1a** to the unoccupied σ^* orbital of H_2. Similarly, forward-bonding is dominated by charge transfer from the σ orbital of H_2 to the LUMO p orbital of **1a**. The difference between back-bonding and forward-bonding charge transfer stabilization of 6.4 kcal/mol is small compared to metal-mediated H_2 activation transition states, which showed up to a difference of ~40 kcal/mol in some cases.[12] This small difference suggests that the (alkyl)(amino)carbene **1a** acts as an ambiphile toward H_2 in the transition state and not a potent nucleophile as previously suggested.[4c] This ambiphilic description is in harmony with the electronic description using the conceptual DFT dual descriptor.[23c,24]

The similar strength of forward-bonding and back-bonding orbital charge transfer stabilization is surprising given the magnitude of the frontier molecular orbital (FMO) energy gaps (Figure 2, top). In **TS1a**, the HOMO of **1a** to H_2 σ^* energy gap is 4.7 eV while the H_2 HOMO to **1a** LUMO energy gap is 10.3 eV. This indicates that while the FMO gap is smallest for back-bonding, this direction of charge flow is hampered by poor orbital overlap in the transition-state geometry. Therefore, analysis of only FMO energy gaps neither provides a reasonable estimate of energy stabilization gained between the interacting fragments in the transition state nor an accurate description of the nucleophilic versus electrophilic character of the carbene. This overlap effect differentiates H_2 activation by ER_2 compounds compared with transition metals where there is often effective overlap in both bonding directions.

ALMO analysis of structures for H_2 approach to **1a** at the extreme geometries shown in Schemes 7a and 7c reveals that the ΔE_{CT1} and ΔE_{CT2} values significantly change as a function of $\theta 1$. When $\theta 1 = 90°$ at a side-on geometry (Scheme 7a), with the H_2 and E−H bond distances and $\theta 2$ fixed at the transition state bond lengths and angle, ΔE_{CT1} decreases to approximately −21 kcal/mol while ΔE_{CT2} increases slightly to approximately −33 kcal/mol (Figure 3a). Here the forward-bonding interaction between the σ orbital of H_2 to the LUMO p orbital of **1a** is the dominant stabilizing interaction mainly because back-bonding has diminished. At the other extreme when $\theta 1 = 180°$ (Scheme 7c), surprisingly ΔE_{CT1} increases in stabilization to approximately −49 kcal/mol, despite the symmetries of the frontier orbitals interacting. Also at $\theta 1 = 180°$, ΔE_{CT2} decreases in stabilization to approximately −19 kcal/mol, presumably because the σ orbital of H_2 is now directed toward the node of the LUMO p orbital of **1a**. In this geometry back-bonding stabilization now significantly dominates.

The analysis in Figure 3a shows that the nucleophilicity of **1a** is highly dependent on the approach angle of H_2 while electrophilicty of **1a** is also affected, but to a lesser extent. Stated another way, orbital overlap from side-on approach enhances net electrophilic carbene character whereas a direct approach enhances overlap for net nucleophilic carbene character. Importantly, analysis of ΔE_{CT1} and ΔE_{CT2} values as a function of $\theta 1$ revealed that the transition state trajectory of H_2 toward **1a** in **TS1a** ($\theta 1 = \sim 130°$) maximizes the sum of ΔE_{CT1} and ΔE_{CT2} values, which is necessary to overcome the closed-shell repulsion upon interaction. Equally important, this transition-state angle of H_2 approach also avoids large Pauli repulsion that occurs at the extreme geometries. Figure 3a shows that at $\theta 1 = 180°$, where the carbene acts most nucleophilic, ΔE_{FRZ} is 144 kcal/mol, which is 50 kcal/mol more destabilizing than in the transition-state geometry. At $\theta 1 = 90°$, ΔE_{FRZ} is equal to 100 kcal/mol, which is 7 kcal/mol more destabilizing than in **TS1a**. ΔE_{FRZ} is at a minimum in the transition-state geometry.

Analysis of electron flow (ΔQ, see Supporting Information), rather than energy stabilization resulting from charge transfer, also shows that in **TS1a** the carbene acts as an ambiphile toward H_2. In **TS1a**, back-bonding charge transfer results in a ΔQ_1 value of 0.105 e while forward-bonding charge transfer results in a ΔQ_2 value of 0.094 e.

The $\Delta E^{\ddagger}$ for **TS1b** of 19.1 kcal/mol is ~4 kcal/mol larger than the barrier for **TS1a**. The distortion and interaction energy values, 28.6 and −9.5 kcal/mol, for this transition state are both larger than in **TS1a**. In **TS1b** the origin of the larger ΔE_{DIST} is the result of a longer H_2 partial bond length. The −9.5 kcal/mol ΔE_{INT} value results from 112.9 kcal/mol destabilizing Pauli repulsion counteracted by −54.0 kcal/mol of stabilizing polarization interactions and −73.5 kcal/mol of stabilizing charge transfer interactions. The charge transfer dissected into back-bonding and forward-bonding shows that $\Delta E_{CT1} = -44.6$ kcal/mol and $\Delta E_{CT2} = -28.9$ kcal/mol. This ΔE_{CT1} value is ~10 kcal/mol more stabilizing than in **TS1a**. The ΔE_{CT2} values in **TS1a** and **TS1b** are almost the same.

Generally, when larger distortion and interaction energies occur in a transition state this is a result of a later transition state position along the reaction coordinate because of less favorable interactions that develop between reacting fragments.[25] One

dx.doi.org/10.1021/ic4010399 | Inorg. Chem. 2013, 52, 8820−8833

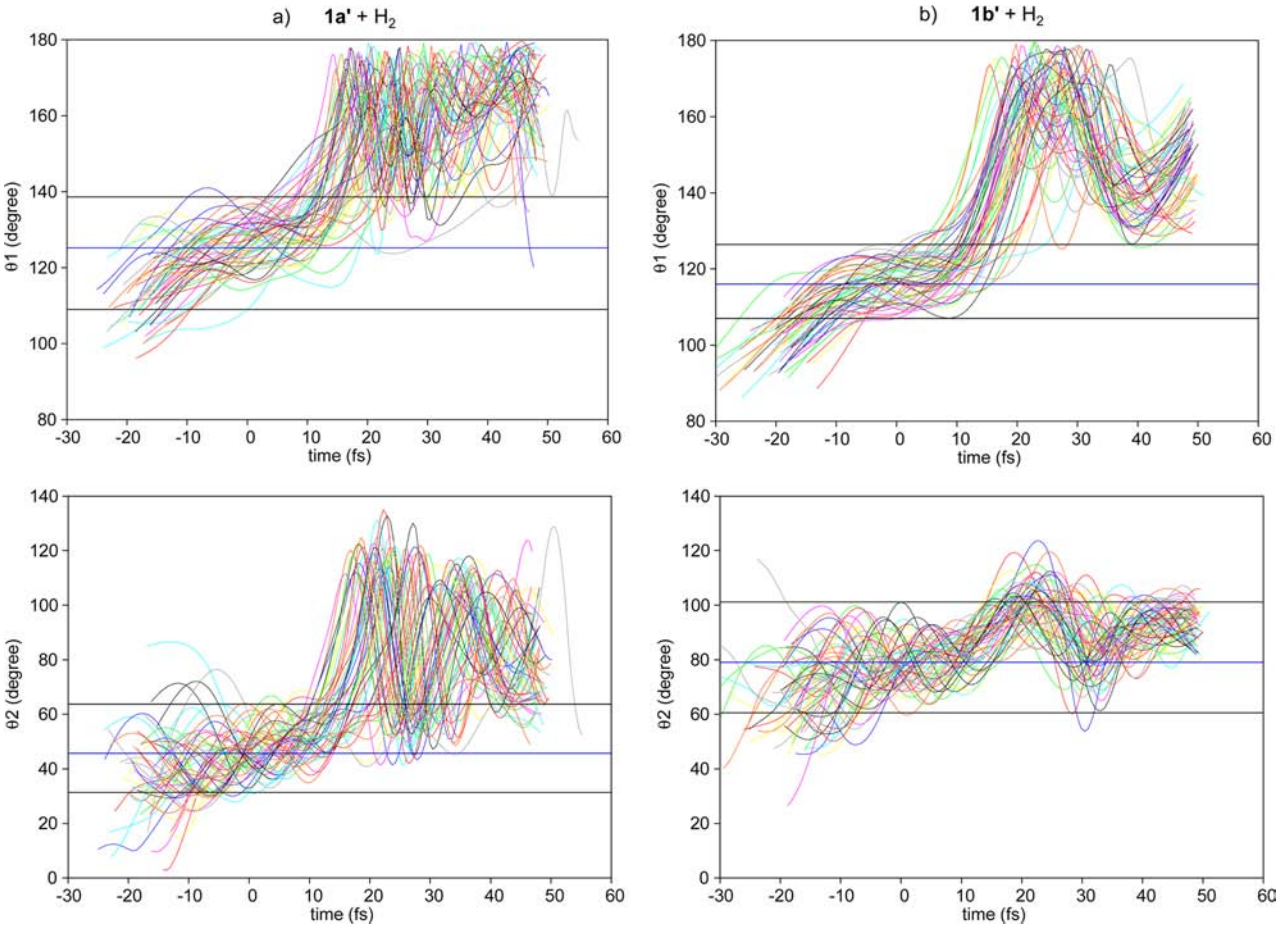

Figure 8. Plot of angles $\theta 1$ and $\theta 2$ during reactive trajectories for H_2 addition to **1a**′ and **1b**′. The transition state is at 0 fs. Negative time leads to reactants and positive time to addition products. The horizontal blue solid lines show the value at the saddle point geometry.

possible explanation for the larger activation barrier in **TS1b** compared to **TS1a** is that the orbital interactions between **1b** and H_2 are less stabilizing than between **1a** and H_2. Inspection of the ground-state FMO energy gaps in Figure 3 shows that the **1b** HOMO to H_2 σ^* back-bonding energy gap is 0.7 eV larger than the back-bonding gap between the ground states of **1a** and H_2. Indeed, this qualitatively suggests a larger activation barrier and slower reaction. However, inspection of the FMO energy gaps in the transition state reveals that the back-bonding energy gap is actually 0.2 eV smaller in **TS1b** than in **TS1a**, which is consistent with the ALMO ΔE_{CT} values.

Why can a transition state with more stabilizing orbital interactions have a larger barrier? The answer is closed-shell repulsion. As H_2 interacts with **1a** or **1b** repulsion occurs between the lone pair and core electrons with the H_2 bond pair electrons. To overcome the closed-shell repulsion the FMO energy gaps adjust by H_2 stretching to narrow its intramolecular HOMO−LUMO energy gap, which decreases the intermolecular FMO energy gaps. In the case of **1b** versus **1a** reacting with H_2, there is larger closed-shell repulsion that results in a larger H_2 partial bond length and larger stabilizing orbital interactions.

The difference in ALMO energy stabilization between forward-bonding and back-bonding interactions in **TS1b** is 14 kcal/mol, which is a much larger difference than found in **TS1a**. Therefore, the divalent silicon compound **1b** imparts more relative and absolute nucleophilic orbital stabilization in the H_2 activation transition state than **1a** in **TS1a**. This result is intriguing since the recent report by Jones, Mountford, Aldrige, and co-workers suggested that divalent Si compounds act as an electrophile when reacting with H_2 since the side-on approach should maximize forward-bonding orbital interaction. As discussed above, the reason why **1b** acts as a more potent nucleophile than **1a** is that the H_2 bond length is stretched to a larger distance in **TS1b** than in **TS1a**. It should be noted that if the geometry-optimized FMO energies were analyzed, **1b** would incorrectly be assigned as less nucleophilic than **1a**. Again, similar to **TS1a**, the FMO energies do not provide accurate estimates of interactions in the transition state because of neglect of closed-shell repulsion and orbital overlap influences.

To examine the effect of orbital overlap due to the angle of H_2 approach to **1b**, ΔE_{CT1} and ΔE_{CT2} values were calculated as a function of $\theta 1$ (Figure 3b). Similar to the interactions between **1a** and H_2, back-bonding stabilization (ΔE_{CT1}) steadily increases from −37 kcal/mol at $\theta 1 = 90°$ to −99 kcal/mol at $\theta 1 = 180°$. In contrast to the interactions between **1a** and H_2 where forward-bonding showed a maximum at $\theta 1 = 90°$ and a minimum at $\theta 1 = 180°$, forward-bonding stabilization between **1b** and H_2 (ΔE_{CT2}) was found to increase from −33 kcal/mol at $\theta 1 = 90°$ to −41 kcal/mol at $\theta 1 = 180°$. If both forward-bonding and back-bonding are maximized at $\theta 1 = 180°$ then why is the $\theta 1$ value in **TS1b** close to 90°?

Inspection of the ΔE_{FRZ} values as a function of $\theta 1$ shows that it is minimized at $\theta 1 = 90°$. This is different than **1a**, which was minimized at approximately $\theta 1 = \sim 120°$ The geometry of **TS1b** is such that H_2 interacts with **1b** from a side-on approach during activation because it minimizes closed-shell electron repulsion.

dx.doi.org/10.1021/ic4010399 | Inorg. Chem. 2013, 52, 8820−8833

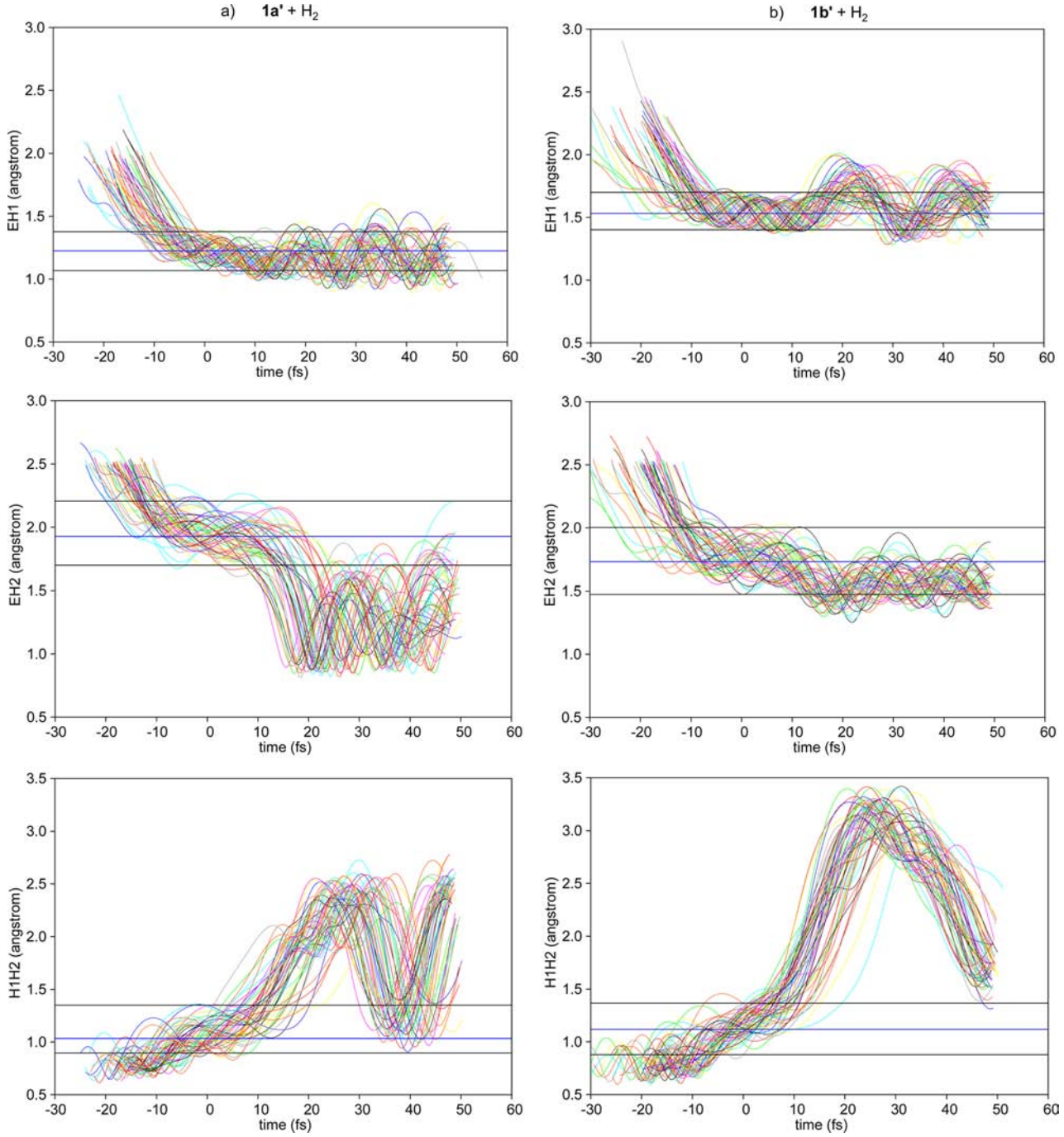

Figure 9. Plot of E−H1, E−H2, and H1−H2 bond lengths during reactive trajectories for H_2 addition to **1a′** and **1b′**. Positive time leads to addition products. The horizontal blue solid lines show the value at the saddle point geometry.

This side-on trajectory is also only possible because back-bonding interactions are not completely diminished.

Analysis of the electron flow (ΔQ, see Supporting Information) in **TS1b** also confirms that the **1b** acts as a nucleophile toward H_2 in the transition state. Back-bonding charge transfer results in a ΔQ_1 value of 0.313 e while forward-bonding charge transfer results in a ΔQ_2 value of 0.064 e.

As suggested by the geometry of **TS1c** the approach of H_2 is similar to **TS1b**, but the H_2 partial bond length is longer. The ALMO analysis reported in Table 1 shows that the interaction energy components of **TS1c** are very similar to the values found in **TS1b**. This suggests that the origin of the larger activation energy (32.4 kcal/mol) is the result of the larger distortion energy, which results from larger intermolecular closed-shell repulsion and worse orbital overlap.

Table 1 also reports the activation energies and ALMO analysis for divalent carbon, Si, and Ge with a computational model of the {B(NDippCH)$_2$}{N-(SiMe$_3$)Dipp}; (Dipp = 2,6-*i*pr$_2$C$_6$H$_3$) ligand reported by Jones and co-workers. The $\Delta E^{\ddagger}$ for **TS2a** is 12.9 kcal/mol. This is 2.5 kcal/mol lower than the barrier for **TS1a**. The barriers for **TS2b** and **TS2c** also have ∼4 kcal/mol lower barriers than **TS1b** and **TS1c**. However, the trend in increase in activation barrier along the series carbon to Si to Ge remains roughly the same as found along the series **1a**, **1b**, and **1c**.

dx.doi.org/10.1021/ic4010399 | *Inorg. Chem.* 2013, 52, 8820−8833

Comparison of the dissected ALMO interaction energy values for transition structures **TS2** versus transition structures **TS1** suggests that the lower barriers are the result of a smaller ΔE_{FRZ} component. This suggests that the R group ligand decreases closed-shell repulsion or potentially increases the Coulombic attraction between ER_2 and H_2 in the transition state.

Main group compounds **3a−c** are similar to compounds **1a−c** except there is a cyclic backbone connecting the alkyl and amino groups. This tied-back alkyl amino group results in the barriers for **TS3** to be 5−17 kcal/mol higher than the barriers for **TS1**. The larger barriers are the result of a later transition state position along the reaction coordinate where the H_2 bond is stretched further and results in 15−20 kcal/mol larger distortion energies. The later transition state position also induces greater interaction energies. The later position of the H_2 activation transition state along the reaction coordinate for compounds **3a−c** also means that these compounds act as more potent nucleophiles toward H_2 than **1a−c**. The difference between back-bonding and forward-bonding ($\Delta E_{CT2} - \Delta E_{CT1}$) stabilization in **TS3** ranges from 18 to 40 kcal/mol. This is larger than the 6−15 kcal/mol range for **TS1** structures.

Reaction Pathway Analysis. To examine the electronic character of the divalent main group compounds interacting with H_2 along the reaction coordinate, Figure 4 plots the ALMO interaction energies along the intrinsic reaction coordinate (IRC) pathway for the reactions of **1a**, **1b**, and **1c**.

Examination of Figure 4a shows that not until the transition state does the ΔE_{INT} between **1a** and H_2 become overall stabilizing. This is due to closed-shell repulsion (ΔE_{FRZ}) because ΔE_{POL} and both ΔE_{CT} values are stabilizing at the early stages of the reaction pathway. Polarization stabilization increases in stability along the reaction coordinate but is quantitatively less important than the charge transfer stabilization energies. Along the reaction pathway the difference between back-bonding and forward-bonding charge transfer stabilization ($\Delta E_{CT2} - \Delta E_{CT1}$) is 4−9 kcal/mol. This is due to both back-bonding and forward-bonding stabilization increasing at approximately the same rate along the reaction pathway.

Similar to the reaction pathway for addition of H_2 to **1a**, the reaction pathway for H_2 activation by **1b** (Figure 4b) shows that ΔE_{INT} is initially destabilizing because of closed-shell repulsion and then becomes stabilizing at the IRC point just prior to the transition-state geometry. Also, ΔE_{POL} and ΔE_{CT} values are always stabilizing along the reaction pathway. The total charge transfer stabilization along the reaction pathways for **1a** and **1b** are similar in magnitude. However, a major difference is that back-bonding and forward-bonding stabilization do not increase at the same rate in the reaction pathway of **1b**. Forward-bonding (ΔE_{CT2}) is slightly more stabilizing than back-bonding (ΔE_{CT1}) at the initial stages of the reaction. At three IRC steps prior to the transition-state geometry ΔE_{CT1} becomes more stabilizing than ΔE_{CT2}. ΔE_{CT1} continues to increase along the reaction coordinate while ΔE_{CT2} increases by only a few kcal/mol. This reaction coordinate suggests that as the reaction progresses toward the H_2 insertion product **1b** acts more nucleophilic.

It is sufficient to comment that the reaction pathways for addition of H_2 to **1c** involves interaction energies that are qualitatively very similar to those of H_2 and **1b**.

Thermodynamics of H_2 Activation. The reaction energies for H_2 addition to compounds **1−3** are reported in Table 1. Comparison of these values with the activation barriers shows a definitive kinetic-thermodynamic relationship. Comparison of compounds **1a**, **1b**, and **1c** show that the addition of H_2 to **1a** is most exothermic with a ΔE_{rxn} value of −66.0 kcal/mol, and this correlates to the lowest $\Delta E^{\ddagger}$ value along this series of compounds. The least exothermic reaction is between **1c** and H_2 with a ΔE_{rxn} value of −25.8 kcal/mol. Previous computational studies have suggested that reaction thermodynamics of carbene and heavier analogues with alkenes and other substrates can be understood based on intramolecular singlet−triplet gaps.[4c,26] The vertical singlet−triplet gaps for **1a**, **1b**, and **1c** are 20.5, 27.0, and 29.1 kcal/mol, respectively. This indeed shows that the smallest singlet−triplet gap is correlated to the most exothermic reaction energy. However, there is no direct quantitative relationship between these singlet−triplet gap energies and the ∼20 kcal/mol decrease in exothermicity going from carbon to Si and then another ∼20 kcal/mol decrease in exothermicity going from Si to Ge.

This suggests that the bond dissociation energies should also provide quantitative insight into the relative reaction thermodynamics. Scheme 9 shows a thermodynamic cycle for H_2 addition to ER_2 involving singlet−triplet excitation followed by formation of the first and then second E−H bond. For **1a**, the first C−H bond dissociation energy is 96 kcal/mol. The second C−H bond dissociation energy is 97 kcal/mol. For **1b** the first and second Si−H bond dissociation energies are 92 and 93 kcal/mol while for **1c** the Ge−H bond dissociation energies are both 86 kcal/mol.[27] Quantitatively, these bond dissociation energies account for approximately half of the reaction energy differences.

Even with consideration of entropic effects the ΔE_{rxn} value for H_2 addition to **1c** is too exothermic for the reaction to be thermodynamically reversible. Divalent compounds **2** and **3** also show similar kinetic-thermodynamic relationships along the carbon to Si to Ge series. Although the ΔE_{rxn} value for the addition of H_2 to compound **3c** is only −10.9 kcal/mol, and might suggest thermodynamic reversibility, the forward and reverse barrier heights are kinetically prohibitive.

Is Reversible H_2 Addition Possible? A broader view of the activation barriers and reaction energies reported in Table 1 suggests that with the right combination of a main group divalent atom center and covalent ligands it might be possible to achieve both a low kinetic barrier and reversible thermodynamic addition of H_2. This would require escaping the kinetic-thermodynamic relationship found for compounds **1−3**. Table 2 reports a systematic examination of activation barriers and reaction thermodynamics for ER_2 compounds where E = C, Si, and Ge and R groups = NH_2, NMe_2, OH, OMe, F, Cl, and Ph.

Examination of the activation barriers in Table 3 shows that for E(H)(R) monosubstituted carbene compounds the barriers range from 13.8 to 1.4 kcal/mol. The largest barriers are found for R = amino and hydroxyl groups while the lowest barriers are found for electron deficient carbenes. Again, there is a general kinetic-thermodynamic relationship where the lowest energy barriers result in the most exothermic H_2 addition products. For example, reaction of monochlorocarbene with H_2 is −106.1 kcal/mol exothermic. Electron withdrawing R groups result in stronger and more polar E−H bonds formed.

As expected from the analysis of compounds **1−3**, alteration of the carbon divalent atom center to Si and Ge increases the activation barriers and reduces the exothermic reaction energies. For monosubstituted E(H)(R) compounds only Ge(H)(Ph) has the potential to react with H_2 kinetically fast and thermodynamically reversible. The activation barrier for this compound is 16.6 kcal/mol, and the reaction energy is −38.6 kcal/mol. All the other monosubstituted E(H)(R) compounds have either

dx.doi.org/10.1021/ic4010399 | Inorg. Chem. 2013, 52, 8820−8833

activation barriers greater than 25 kcal/mol or reaction energies more exothermic than −45 kcal/mol.

Table 2 also reports the activation barriers and reaction energies for $E(R)_2$ disubstituted compounds. When the R groups are both π donors the activation energies are larger than 25 kcal/mol. For example, $C(NH_2)_2$ has an activation barrier of 32.6 kcal/mol. This is more than a 19 kcal/mol increase in barrier height compared to $C(H)(NH_2)$. This large barrier also accounts for why Bertrand and co-workers observed no activation of H_2 by di(amino)carbenes.[4c] The reaction energy also becomes less exothermic by more than 25 kcal/mol.

In contrast to the di(amino)carbenes, dimethyl carbene $C(CH_3)_2$ has an activation barrier of only 2.3 kcal/mol. This shows that the activation barrier is significantly influenced by the degree of π donor ability of the R groups. As expected, the reaction energy of dimethyl carbene and H_2 is more than 100 kcal/mol exothermic.

To test to the effects of π acceptor groups, the activation energy and reaction energy was computed for $C(BH_2)_2$. The activation barrier is low and ∼8 kcal/mol. The reaction energy is −50.7 kcal/mol. This is more than 50 kcal/mol less exothermic than for dimethyl carbene and only a few kcal/mol more exothermic than for diamino carbene. This result suggests that the ideal combination for a low barrier and thermoneutral reaction energy involves R groups with a balance of electropositive σ donor and poor π donor groups.

Closer to the ideal situation is found for $Ge(BH_2)_2$. The activation barrier for this compound is 6.3 kcal/mol and the reaction energy is −23.8 kcal/mol. This compound, or similar variants, has the possibility for an increase in activation barrier with a decrease in reaction energy that could give a desired barrier around 15 kcal/mol and reaction energy of no greater than −10 kcal/mol.

Quasiclassical Trajectories (QCT) of H_2 Activation. The differences among the transition structures for H_2 addition to divalent C, Si, and Ge raise an important dynamical question: where do these reactions lie on the spectrum of concerted versus stepwise addition? The IRCs in the Supporting Information and Figure 4 suggest concerted addition, but ample precedent exists for dynamical exploration of non-IRC pathways.[28] QCT calculations were used to compute the dynamics and the distribution of E−H bond formation times in these addition reactions.

In Wang and Karplus's pioneering CNDO trajectory study of CH_2 with H_2,[13e] they found a very wide and complex range of trajectory motions centered approximately around the minimum energy path. Recently, Xu et al. have reported quasiclassical trajectory calculations for CCl_2 and CF_2 addition to ethylene.[29] With a modified version of B3LYP with reduced HF exchange, they found that all trajectories follow a nonleast-motion pathway. The average time between the first and second C−C bond formation averages 50 fs but can be as high as 250 fs. These bond forming time gaps are longer than those computed for 1,3-dipolar and Diels−Alder cycloadditions.[30]

A total of 128 quasiclassical trajectories were calculated: 64 trajectories for the reaction between **1a′** and H_2 and 64 trajectories for reaction between **1b′** and H_2. **1a′** and **1b′** (Scheme 5) are model compounds for **1a**, **1b**, **3a**, and **3b**. Trajectories were also calculated for reaction of **1c′** with H_2 but are highly similar to the reaction between **1b′** and H_2 and so are not reported here. Figure 5 shows overlays of the sampled transition-state geometries for each set of 64 trajectories. In the sample geometries for addition of H_2 to **1a′** the angles θ1 and θ2 range between 109 and 139° and 31−64°. For the addition of H_2 to **1b′** the angles θ1 and θ2 range between 107 and 127° and 61−101°. Defined in Scheme 7, θ1 and θ2 values provide a convenient view of the approach and reaction of H_2 with the ER_2 species.

Figures 6 and 7 show sample reaction trajectories for H_2 activation by **1a′** and **1b′**. The trajectory shown in Figure 6 involves an initial linear H_2 approach toward the empty p orbital of the carbon atom 14 fs before the transition state and then tilts to interact with carbon a few femtoseconds later. In contrast, the trajectory shown in Figure 7 begins with a side-on interaction with θ1 and θ2 close to 90° from 24 fs until the transition state region. It is not until after the transition state and with significant Si−H bond formation that the H_2 tilts to interact with the Si atom center.

Figure 8 plots the trajectory patterns for H_2 approach and reaction with **1a′** and **1b′** by monitoring angles θ1 and θ2 versus time. Negative time leads to reactants, positive time to products, and time 0 is the sampled transition state point. Trajectories start between −30 to −20 fs (reactant side) and pass through the saddle point at 0 fs and the products are formed at approximately 50 fs (product side). The trajectories of H_2 addition to **1a′** show that the approach of H_2, as measured by θ1, increases slowly until the saddle point region and then increases sharply around 10 fs after the transition state because of H_2 bond cleavage. This is because H_2 bonding stretching in the transition state immediately becomes bending modes in the addition product and their motion is coupled. A similar situation was found for the θ1 values of H_2 addition to **1b′**. In the carbene trajectories, θ1 reaches a maximum around 15 fs and then fluctuates between 180° and 140°. In the silylene trajectories, θ1 reaches maximum at a slightly longer time period, estimated between 15−30 fs after the transition state. Again, once the addition product is formed θ1 values show significant fluctuation, but not as significant as carbene trajectories.

Interestingly, the trajectory calculations reveal that there is a rather wide range of θ1 values for the initial approach of H_2 to react with **1a′**. This is likely due to the very small overall stabilizing interaction energy between fragments that is not highly directional. At approximately 20 fs before the transition state many of trajectories have θ1 values close to 110°. The maximum θ1 value calculated for this set of trajectories is ∼140°. The transition state has a similar distribution of θ1 values. These calculations suggest that many of the reaction pathways for H_2 approach to **1a′** involve trajectories similar to what is expected for the reaction between H_2 with **1b′**. Inspection of the trajectories for **1b′** shows that in the early stages of the reaction at ∼20 fs before the transition state H_2 approaches **1b′** from a direct side-on trajectory. At the time of the transition state θ1 values range from 110° and 125°. This is much smaller range of θ1 values than what was found in the reaction with **1a′**.

For θ2, in the carbene trajectories this angle ranges between 10° to 80° on the reactant side but narrows to approximately 35° to 60° at the saddle point and then similar to θ1 fluctuates significantly in the product. For the silylene trajectories, θ2 ranges between 40° and 100° on the reactant side and reaches a maximum value of about 110° within 15−25 fs after crossing the transition state.

Figure 9 plots the E−H1, E−H2, and H1−H2 bond lengths during the calculated trajectories. For H_2 addition to **1a′**, the C−H1 bond is formed first and completely formed at a time range of 3−25 fs after the transition state. The C−H2 bond is formed second during the time frame of 13−48 fs after the transition

dx.doi.org/10.1021/ic4010399 | Inorg. Chem. 2013, 52, 8820−8833

state. The time gap between formation of C−H1 and C−H2 bonds is between 4 and 45 fs (Table 3). Interestingly, the Si−H1 bond in many of the H_2 addition to **1b′** trajectories shows almost complete formation at around −5 fs even before crossing the transition state. The timing of Si−H1 bond formation from these trajectories was found to be in the range of −10 to 28 fs. For the Si−H2 bond, complete formation occurs at 10−20 fs after crossing the transition state. This results in a time gap of Si−H bonds forming between 6 and 58 fs. This lagging of the second Si−H2 bond in comparison to the Si−H1 bond results in a larger average time gap of 21 fs compared to the C−H average time gap of only 11 fs. However, both of these time gaps are shorter than what has been reported for carbene addition to alkenes. This suggests that these reactions occur in a single, dynamically concerted step where the bond forming occurs in less time than the bond vibration.

Table 3. Time Gap of Bond Formation in Trajectories

	bond formation range (fs)	average time for bond formation (fs)
1a′ + H_2		
time gap of bond formation	4−45	11
1b′ + H_2		
time gap of bond formation	6−58	21

The extent of H1−H2 bond cleavage along the trajectories provides insight into the activation process. Although there was a difference in time gap of forming the E−H bonds for **1a′** and **1b′**, the extent to which the H1−H2 bond is cleaved is remarkably similar. For **1a′**, H1−H2 bond is fully broken 10−20 fs after crossing the transition state and for **1b′** this bond is broken 5−15 fs after the transition state. These trajectories also revealed that during the course of reaction the relative position of the atom H2 in H_2 does not change significantly compared to H1 because the N−C/Si−C−H2 dihedral angle remains nearly constant throughout the trajectories (see Supporting Information). In contrast, the dihedral angle N−C/Si−C−H1 changes synchronously with increase in the H1−H2 bond length as each trajectory progresses.

CONCLUSION

A comprehensive picture of H_2 addition to carbon, Si, and Ge singlet divalent main group compounds has been provided by a combination of DFT and quasiclassical trajectories. Calculations have shown the following:

(1) The majority of the activation barrier for concerted H_2 addition to divalent ER_2 compounds results from the energy penalty to stretch H_2 and this is controlled by intermolecular electron repulsion. Electron repulsion also explains the increase in activation barriers and trends in transition-state interactions along the carbon to Si to Ge series.

(2) Divalent (alkyl)(amino)carbene acts as an ambiphile while divalent Si and Ge divalent compounds act as nucleophiles toward H_2 in the transition state. The FMO energy gaps do not provide a reasonable estimate of energy stabilization gained between the interacting fragments in the transition state or an accurate description of the nucleophilic versus electrophilic character. This is because the FMO approximation neglects electron repulsion and orbital overlap influences.

(3) In CR_2 transition states forward-bonding and back-bonding are maximized in the nonleast-motion geometry. In contrast, SiR_2/GeR_2 transition states have side-on geometries to avoid electron repulsion.

(4) Examination of barrier heights and reaction energies shows a clear kinetic-thermodynamic relationship for ER_2 activation of H_2. A survey of barriers and reaction energies for ER_2 compounds suggests that the ideal combination for a low barrier and thermoneutral reaction energy involves R groups that balance an electropositive σ donor with a poor π donor group.

(5) QCTs show that dihydrogen approach and reaction with CR_2 may involve geometries significantly different than the static transition-state structure suggests. In contrast, dihydrogen addition to SiR_2 involves geometries close to the side-on approach suggested by the static transition-state structure.

(6) QCTs also demonstrate that addition of H_2 to CR_2 and SiR_2 is dynamically concerted.

ASSOCIATED CONTENT

Supporting Information

Full references 15 and 16, (U)B3LYP and UCCSD(T) IRC plots, singlet−triplet gap energies, activation, and reaction energies of **1a′**, **1b′**, and **1c′** addition to H_2, ALMO-EDA of transition states reported in Table 2, and plots of the dihedral angles N-E−C−H1/H2 in trajectories. This material is available free of charge via the Internet at http://pubs.acs.org.

AUTHOR INFORMATION

Corresponding Author

*E-mail: dhe@chem.byu.edu (D.H.E.), ced3@columbia.edu (C.E.D.).

Notes

The authors declare no competing financial interest.

ACKNOWLEDGMENTS

D.H.E. thanks Brigham Young University (BYU) and the Fulton Supercomputing Lab (FSL) for support. Acknowledgment is made to the Donors of the American Chemical Society Petroleum Research Fund for support to D.H.E (51081-DNI3). D.H.E. also thanks XSEDE for a start-up allocation. C.D. thanks the National Science Foundation for support, CHE-0910876 and CHE-1213976, and XSEDE, supported by NSF OCI-1053575, for computer resources.

REFERENCES

(1) (a) Tye, J. W.; Darensbourg, M. Y.; Hall, M. B. The Activation of Dihydrogen. In *Activation of Small Molecules: Organometallic and Bioinorganic Perspectives*; Tolman, W. B., Ed.; Wiley-VCH: Weinheim, Germany, 2006; p 121. (b) Crabtree, R. H. *The Organometallic Chemistry of the Transition Metals*, 5th ed.; John Wiley & Sons: New York, 2005. (c) Kubas, G. J. *Metal-Dihydrogen and σ-Bond Complexes: Structure, Bonding, and Reactivity*; Kluwer Academic/Plenum Publishers: New York, 2001. (d) Frey, M. *ChemBioChem* **2002**, *3*, 153.

(2) (a) Kubas, G. J. *Science* **2006**, *314*, 1096. (b) Kenward, A. L.; Piers, W. E. *Angew. Chem., Int. Ed.* **2008**, *47*, 38. (c) Driess, M. *Nat. Chem.* **2012**, *4*, 525. (d) Power, P. P. *Nature* **2010**, *463*, 171. (e) Erős, G.; Mehdi, H.; Pápai, I.; Rokob, T. A.; Király, P.; Tárkányi, G.; Soós, T. *Angew. Chem., Int. Ed.* **2010**, *49*, 6559.

(3) (a) Xiao, Z. L.; Hauge, R. H.; Margrave, J. L. *Inorg. Chem.* **1993**, *32*, 642. (b) Kötting, C.; Sander, W. *J. Am. Chem. Soc.* **1999**, *121*, 8891. (c) Himmel, H.-J.; Vollet, J. *Organometallics* **2002**, *21*, 5972. (d) Berkessel, A.; Schubert, T. J. S.; Müller, T. N. *J. Am. Chem. Soc.* **2002**, *124*, 8693. (e) Spikes, G. H.; Fettinger, J. C.; Power, P. P. *J. Am. Chem. Soc.* **2005**, *127*, 12232. (f) Zhao, L.; Huang, F.; Lu, G.; Wang, Z.-

X.; Schleyer, P. v. R. *J. Am. Chem. Soc.* **2012**, *134*, 8856. (g) Power, P. P. *Acc. Chem. Res.* **2011**, *44*, 627. (h) Peng, Y.; Brynda, M.; Ellis, B. D.; Fettinger, J. C.; Rivard, E.; Power, P. P. *Chem. Commun. (Cambridge, U. K.)* **2008**, 6042. (i) Zhu, Z.; Wang, X.; Peng, Y.; Lei, H.; Fettinger, J. C.; Rivard, E.; Power, P. P. *Angew. Chem., Int. Ed.* **2009**, *48*, 2031. (j) Li, J.; Schenk, C.; Goedecke, C.; Frenking, G.; Jones, C. *J. Am. Chem. Soc.* **2011**, *133*, 18622.

(4) (a) Peng, Y.; Ellis, B. D.; Wang, X. P.; Power, P. P. *J. Am. Chem. Soc.* **2008**, *130*, 12268. (b) Peng, Y.; Guo, J. D.; Ellis, B. D.; Zhu, Z. L.; Fettinger, J. C.; Nagase, S.; Power, P. P. *J. Am. Chem. Soc.* **2009**, *131*, 16272. (c) Frey, G. D.; Lavallo, V.; Donnadieu, B.; Schoeller, W. W.; Bertrand, G. *Science* **2007**, *316*, 439. (d) Protchenko, A. V.; Birjkumar, K. H.; Dange, D.; Schwarz, A. D.; Vidovic, D.; Jones, C.; Kaltsoyannis, N.; Mountford, P.; Aldridge, S. *J. Am. Chem. Soc.* **2012**, *134*, 6500. (e) Protchenko, A. V.; Schwarz, A. D.; Blake, M. P.; Jones, C.; Kaltsoyannis, N.; Mountford, P.; Aldridge, S. *Angew. Chem.* **2013**, *125*, 596.

(5) (a) Welch, G. C.; Cabrera, L.; Chase, P. A.; Hollink, E.; Masuda, J. D.; Wei, P.; Stephan, D. W. *Dalton Trans.* **2007**, *0*, 3407. (b) Welch, G. C.; Juan, R. R. S.; Masuda, J. D.; Stephan, D. W. *Science* **2006**, *314*, 1124. (c) Stephan, D. W. *Org. Biomol. Chem.* **2008**, *6*, 1535. (d) Stephan, D. W. *Dalton Trans.* **2009**, 3129. (e) Welch, G. C.; Stephan, D. W. *J. Am. Chem. Soc.* **2007**, *129*, 1880. (f) Li, H.; Zhao, L.; Lu, G.; Mo, Y.; Wang, Z.-X. *Phys. Chem. Chem. Phys.* **2010**, *12*, 5268. (g) Stephan, D. W.; Erker, G. *Angew. Chem., Int. Ed.* **2010**, *49*, 46. (h) Rokob, T. A.; Hamza, A.; Stirling, A.; Soós, T.; Pápai, I. *Angew. Chem., Int. Ed.* **2008**, *47*, 2435. (i) Farrell, J. M.; Hatnean, J. A.; Stephan, D. W. *J. Am. Chem. Soc.* **2012**, *134*, 15728. (j) Könczöl, L.; Makkos, E.; Bourissou, D.; Szieberth, D. *Angew. Chem., Int. Ed.* **2012**, *51*, 9521. (k) Rokob, T. A.; Hamza, A.; Stirling, A.; Soós, T.; Pápai, I. *Angew. Chem.* **2008**, *120*, 2469. (l) Rajeev, R.; Sunoj, R. B. *Chem.—Eur. J.* **2009**, *15*, 12846. (m) Grimme, S.; Kruse, H.; Goerigk, L.; Erker, G. *Angew. Chem., Int. Ed.* **2010**, *49*, 1402. (n) Kenward, A. L.; Piers, W. E. *Angew. Chem., Int. Ed.* **2008**, *47*, 38. (o) Erker, G. *C. R. Chim.* **2011**, *14*, 831. (p) Stephan, D. W.; Greenberg, S.; Graham, T. W.; Chase, P.; Hastie, J. J.; Geier, S. J.; Farrell, J. M.; Brown, C. C.; Heiden, Z. M.; Welch, G. C.; Ullrich, M. *Inorg. Chem.* **2011**, *50*, 12338. (q) Stephan, D. W. *Org. Biomol. Chem.* **2012**, *10*, 5740. (r) Erker, G. *Dalton Trans.* **2011**, *40*, 7475. (s) Erker, G. *Organometallics* **2011**, *30*, 358. (t) Rokob, T. A.; Bakó, I.; Stirling, A.; Hamza, A.; Pápai, I. *J. Am. Chem. Soc.* **2013**, *135*, 4425.

(6) (a) Sumerin, V.; Chernichenko, K.; Nieger, M.; Leskela, M.; Rieger, B.; Repo, T. *Adv. Synth. Catal.* **2011**, *353*, 2093. (b) Schulz, F.; Sumerin, V.; Leskela, M.; Repo, T.; Rieger, B. *Dalton Trans.* **2010**, *39*, 1920. (c) Sumerin, V.; Schulz, F.; Nieger, M.; Atsumi, M.; Wang, C.; Leskela, M.; Pyykko, P.; Repo, T.; Rieger, B. *J. Organomet. Chem.* **2009**, *694*, 2654. (d) Sumerin, V.; Schulz, F.; Atsumi, M.; Wang, C.; Nieger, M.; Leskela, M.; Repo, T.; Pyykko, P.; Rieger, B. *J. Am. Chem. Soc.* **2008**, *130*, 14117. (e) Schulz, F.; Sumerin, V.; Heikkinen, S.; Pedersen, B.; Wang, C.; Atsumi, M.; Leskela, M.; Repo, T.; Pyykko, P.; Petry, W.; Rieger, B. *J. Am. Chem. Soc.* **2011**, *133*, 20245. (f) Grant, D. J.; Dixon, D. A.; Camaioni, D.; Potter, R. G.; Christe, K. O. *Inorg. Chem.* **2009**, *48*, 8811. (g) Runyon, J. W.; Steinhof, O.; Dias, H. V. R.; Calabrese, J. C.; Marshall, W. J.; Arduengo, A. J. *Aust. J. Chem.* **2011**, *64*, 1165. (h) Sumerin, V.; Schulz, F.; Nieger, M.; Leskelä, M.; Repo, T.; Rieger, B. *Angew. Chem., Int. Ed.* **2008**, *47*, 6001. (i) Matus, M. H.; Anderson, K. D.; Camaioni, D. M.; Autrey, S. T.; Dixon, D. A. *J. Phys. Chem. A* **2007**, *111*, 4411. (j) Parvanov, V. M.; Schenter, G. K.; Hess, N. J.; Daemen, L. L.; Hartl, M.; Stowe, A. C.; Camaioni, D. M.; Autrey, T. *Dalton Trans.* **2008**, *0*, 4514. (k) Karkamkar, A.; Parab, K.; Camaioni, D. M.; Neiner, D.; Cho, H.; Nielsen, T. K.; Autrey, T. *Dalton Trans.* **2013**, *42*, 615. (l) Camaioni, D. M.; Ginovska-Pangovska, B.; Schenter, G. K.; Kathmann, S. M.; Autrey, T. *J. Phys. Chem. A* **2012**, *116*, 7228.

(7) (a) Jiang, C.; Blacque, O.; Fox, T.; Berke, H. *Dalton Trans.* **2011**, *40*, 1091. (b) Jiang, C.; Blacque, O.; Berke, H. *Chem. Commun. (Cambridge, U. K.)* **2009**, *0*, 5518. (c) Holschumacher, D.; Bannenberg, T.; Hrib, C. G.; Jones, P. G.; Tamm, M. *Angew. Chem.* **2008**, *120*, 7538. (d) Jiang, C. F.; Blacque, O.; Berke, H. *Organometallics* **2009**, *28*, 5233. (e) Reddy, J. S.; Xu, B.-H.; Mahdi, T.; Fröhlich, R.; Kehr, G.; Stephan, D. W.; Erker, G. *Organometallics* **2012**, *31*, 5638. (f) Inés, B.; Palomas, D.; Holle, S.; Steinberg, S.; Nicasio, J. A.; Alcarazo, M. *Angew. Chem., Int. Ed.* **2012**, *51*, 12367. (g) Jiang, C.; Blacque, O.; Fox, T.; Berke, H. *Organometallics* **2011**, *30*, 2117. (h) Bertini, F.; Lyaskovskyy, V.; Timmer, B. J. J.; de Kanter, F. J. J.; Lutz, M.; Ehlers, A. W.; Slootweg, J. C.; Lammertsma, K. *J. Am. Chem. Soc.* **2012**, *134*, 201. (i) Eisenstein, O.; Crabtree, R. H. *New J. Chem.* **2013**, *37*, 21. (j) Lu, Z.; Cheng, Z.; Chen, Z.; Weng, L.; Li, Z. H.; Wang, H. *Angew. Chem., Int. Ed.* **2011**, *50*, 12227. (k) Piers, W. E.; Marwitz, A. J. V.; Mercier, L. G. *Inorg. Chem.* **2011**, *50*, 12252.

(8) (a) Ghattas, G.; Chen, D.; Pan, F.; Klankermayer, J. *Dalton Trans.* **2012**, *41*, 9026. (b) Marwitz, A. J. V.; Dutton, J. L.; Mercier, L. G.; Piers, W. E. *J. Am. Chem. Soc.* **2011**, *133*, 10026. (c) Greb, L.; Ona-Burgos, P.; Kubas, A.; Falk, F. C.; Breher, F.; Fink, K.; Paradies, J. *Dalton Trans.* **2012**, *41*, 9056. (d) Greb, L.; Oña-Burgos, P.; Schirmer, B.; Grimme, S.; Stephan, D. W.; Paradies, J. *Angew. Chem., Int. Ed.* **2012**, *51*, 10164. (e) Herrington, T. J.; Thom, A. J. W.; White, A. J. P.; Ashley, A. E. *Dalton Trans.* **2012**, *41*, 9019. (f) Kronig, S.; Theuergarten, E.; Holschumacher, D.; Bannenberg, T.; Daniliuc, C. G.; Jones, P. G.; Tamm, M. *Inorg. Chem.* **2011**, *50*, 7344. (g) Lindqvist, M.; Sarnela, N.; Sumerin, V.; Chernichenko, K.; Leskela, M.; Repo, T. *Dalton Trans.* **2012**, *41*, 4310. (h) Mahdi, T.; Heiden, Z. M.; Grimme, S.; Stephan, D. W. *J. Am. Chem. Soc.* **2012**, *134*, 4088. (i) Ménard, G.; Stephan, D. W. *Angew. Chem., Int. Ed.* **2012**, *51*, 8272. (j) Schäfer, A.; Reißmann, M.; Schäfer, A.; Saak, W.; Haase, D.; Müller, T. *Angew. Chem., Int. Ed.* **2011**, *50*, 12636. (k) Travis, A. L.; Binding, S. C.; Zaher, H.; Arnold, T. A. Q.; Buffet, J.-C.; O'Hare, D. *Dalton Trans.* **2013**, *42*, 2431. (l) Caputo, C. B.; Geier, S. J.; Winkelhaus, D.; Mitzel, N. W.; Vukotic, V. N.; Loeb, S. J.; Stephan, D. W. *Dalton Trans.* **2012**, *41*, 2131. (m) Chapman, A. M.; Haddow, M. F.; Wass, D. F. *J. Am. Chem. Soc.* **2011**, *133*, 18463. (n) Bender, G.; Kehr, G.; Daniliuc, C. G.; Dao, Q. M.; Ehrlich, S.; Grimme, S.; Erker, G. *Chem. Commun. (Cambridge, U. K.)* **2012**, *48*, 11085. (o) Bouhadir, G.; Amgoune, A.; Bourissou, D. Chapter 1 - Phosphine-Boranes and Related Ambiphilic Compounds: Synthesis, Structure, and Coordination to Transition Metals. In *Advances in Organometallic Chemistry*; Anthony, F. H., Mark, J. F., Eds.; Academic Press: New York, 2010; Vol. *58*, p 1. (p) Bako, I.; Stirling, A.; Balint, S.; Papai, I. *Dalton Trans.* **2012**, *41*, 9023. (q) Hamza, A.; Stirling, A.; András Rokob, T.; Pápai, I. *Int. J. Quantum Chem.* **2009**, *109*, 2416. (r) Schirmer, B.; Grimme, S. *Chem. Commun. (Cambridge, U. K.)* **2010**, *46*, 7942.

(9) (a) Janowicz, A. H.; Bergman, R. G. *J. Am. Chem. Soc.* **1983**, *105*, 3929. (b) Goldman, A. S.; Goldberg, K. I. Organometallic C-H Bond Activation: An Introduction. In *Activation and Functionalization of C-H Bonds*; American Chemical Society: Washington, DC, 2004; Vol. *885*, p 1.

(10) (a) Hoffmann, R. *Angew. Chem., Int. Ed. Engl.* **1982**, *21*, 711. (b) Fukui, K. *Angew. Chem., Int. Ed. Engl.* **1982**, *21*, 801.

(11) Frey, G. D.; Masuda, J. D.; Donnadieu, B.; Bertrand, G. *Angew. Chem., Int. Ed.* **2010**, *49*, 9444.

(12) Devarajan, D.; Ess, D. H. *Inorg. Chem.* **2012**, *51*, 6367.

(13) (a) Hoffmann, R.; Gleiter, R.; Mallory, F. B. *J. Am. Chem. Soc.* **1970**, *92*, 1460. (b) Hoffmann, R. *J. Am. Chem. Soc.* **1968**, *90*, 1475. (c) Kollmar, H. *Tetrahedron* **1972**, *28*, 5893. (d) Bauschlicher, C. W.; Haber, K.; Schaefer, H. F.; Bender, C. F. *J. Am. Chem. Soc.* **1977**, *99*, 3610. (e) Wang, I. S. Y.; Karplus, M. *J. Am. Chem. Soc.* **1973**, *95*, 8160. (f) Kollmar, H. *J. Am. Chem. Soc.* **1978**, *100*, 2660.

(14) Ess, D. H.; Goddard, W. A.; Periana, R. A. *Organometallics* **2010**, *29*, 6459.

(15) (a) Frisch, M. J., et al. *Gaussian 03*, Revision D.01; Gaussian, Inc.: Wallingford, CT, 2004. (b) Frisch, M. J., et al. *Gaussian 09*, Revision B.01; Gaussian, Inc.: Wallingford, CT, 2010.

(16) Shao, Y., et al. *Q-Chem*, Version 3.2; Q-Chem, Inc.: Pittsburgh, PA.

(17) (a) Khaliullin, R. Z.; Cobar, E. A.; Lochan, R. C.; Bell, A. T.; Head-Gordon, M. *J. Phys. Chem. A* **2007**, *111*, 8753. (b) Khaliullin, R. Z.; Bell, A. T.; Head-Gordon, M. *J. Chem. Phys.* **2008**, *128*, 184112.

(18) (a) Morokuma, K. *J. Chem. Phys.* **1971**, *55*, 1236. (b) Ziegler, T.; Rauk, A. *Inorg. Chem.* **1979**, *18*, 1755. (c) Bickelhaupt, F. M.; Ziegler, T. *Organometallics* **1995**, *14*, 2288. (d) Bickelhaupt, F. M. *J. Comput. Chem.* **1999**, *20*, 114. (e) Ess, D. H.; Houk, K. N. *J. Am. Chem. Soc.* **2007**, *129*,

10646. (f) Ess, D. H.; Houk, K. N. *J. Am. Chem. Soc.* **2008**, *130*, 10187. (g) Diefenbach, A.; de Jong, G. T.; Bickelhaupt, F. M. *J. Chem. Theory Comput.* **2005**, *1*, 286. (h) Cobar, E. A.; Khaliullin, R. Z.; Bergman, R. G.; Head-Gordon, M. *Proc. Natl. Acad. Sci. U. S. A.* **2007**, *104*, 6963. (i) Maseras, F.; Li, X. K.; Koga, N.; Morokuma, K. *J. Am. Chem. Soc.* **1993**, *115*, 10974. (j) Engels, B.; Christl, M. *Angew. Chem., Int. Ed.* **2009**, *48*, 7968.

(19) Hase, W. L.; Duchovic, R. J.; Hu, X.; Lim, K.; Lu, D.-h.; Peslherbe, G. H.; Swamy, K. N.; VandeLinde, S. R.; Wang, H.; Wolfe, R. J. *VENUS 96, a General Chemical Dynamics Computer Program*; QCPE-671, 1996.

(20) (a) Chapman, S.; Bunker, D. L. *J. Chem. Phys.* **1975**, *62*, 2890. (b) Peslherbe, G. H.; Wang, H.; Hase, W. L. Monte Carlo Sampling for Classical Trajectory Simulations. In *Advances in Chemical Physics*; John Wiley & Sons, Inc.: New York, 2007; p 171. (c) Doubleday, C.; Bolton, K.; Hase, W. L. *J. Phys. Chem. A* **1998**, *102*, 3648.

(21) de Jong, G. T.; Bickelhaupt, F. M. *J. Chem. Theory Comput.* **2006**, *2*, 322.

(22) (a) Fischer, R. C.; Power, P. P. *Chem. Rev.* **2010**, *110*, 3877. (b) Lein, M.; Krapp, A.; Frenking, G. *J. Am. Chem. Soc.* **2005**, *127*, 6290. (c) Kutzelnigg, W. *Angew. Chem., Int. Ed. Engl.* **1984**, *23*, 272. (d) Lattanzi, V.; Thorwirth, S.; Halfen, D. T.; Mück, L. A.; Ziurys, L. M.; Thaddeus, P.; Gauss, J.; McCarthy, M. C. *Angew. Chem., Int. Ed.* **2010**, *49*, 5661. (e) Devarajan, D.; Frenking, G. *Chem.—Asian J.* **2012**, *7*, 1296.

(23) (a) Toro-Labbé, A.; Gutiérrez-Oliva, S.; Murray, J. S.; Politzer, P. *Mol. Phys.* **2007**, *105*, 2619. (b) Burda, J. V.; Murray, J. S.; Toro-Labbé, A.; Gutiérrez-Oliva, S.; Politzer, P. *J. Phys. Chem. A* **2009**, *113*, 6500. (c) Duarte, F.; Toro-Labbé, A. *J. Phys. Chem. A* **2011**, *115*, 3050. (d) Vöhringer-Martinez, E.; Toro-Labbé, A. *J. Phys. Chem. A* **2012**, *116*, 7419. (e) Labet, V.; Morell, C.; Grand, A.; Toro-Labbé, A. *J. Phys. Chem. A* **2008**, *112*, 11487.

(24) (a) Geerlings, P.; De Proft, F.; Langenaeker, W. *Chem. Rev.* **2003**, *103*, 1793. (b) Morell, C.; Grand, A.; Toro-Labbé, A. *J. Phys. Chem. A* **2004**, *109*, 205.

(25) Ess, D. H. *J. Org. Chem.* **2009**, *74*, 1498.

(26) (a) Wang, Y.; Ma, J. *J. Organomet. Chem.* **2009**, *694*, 2567. (b) Mendez, F.; Garcia-Garibay, M. A. *J. Org. Chem.* **1999**, *64*, 7061. (c) Amani, J.; Musavi, S. M.; Riazikia, M. *Organometallics* **2012**, *31*, 4157. (d) Rondan, N. G.; Houk, K. N.; Moss, R. A. *J. Am. Chem. Soc.* **1980**, *102*, 1770. (e) Moss, R. A. *Acc. Chem. Res.* **1980**, *13*, 58. (f) Bach, R. D.; Su, M. D.; Aldabbagh, E.; Andres, J. L.; Schlegel, H. B. *J. Am. Chem. Soc.* **1993**, *115*, 10237. (g) Mieusset, J.-L.; Brinker, U. H. *J. Org. Chem.* **2008**, *73*, 1553. (h) Gronert, S.; Keeffe, J. R.; More O'Ferrall, R. A. *J. Org. Chem.* **2009**, *74*, 5250. (i) Wu, C. S.; Su, M. D. *Dalton Trans.* **2012**, *41*, 3253.

(27) van Stralen, J. N. P.; Bickelhaupt, F. M. *Organometallics* **2006**, *25*, 4260.

(28) (a) Doubleday, C. *J. Phys. Chem. A* **2001**, *105*, 6333. (b) Sun, L. P.; Song, K. Y.; Hase, W. L. *Science* **2002**, *296*, 875. (c) Ammal, S. C.; Yamataka, H.; Aida, M.; Dupuis, M. *Science* **2003**, *299*, 1555. (d) Carpenter, B. K. *Annu. Rev. Phys. Chem.* **2005**, *56*, 57. (e) Lopez, J. G.; Vayner, G.; Lourderaj, U.; Addepalli, S. V.; Kato, S.; Dejong, W. A.; Windus, T. L.; Hase, W. L. *J. Am. Chem. Soc.* **2007**, *129*, 9976. (f) Bekele, T.; Christian, C. F.; Lipton, M. A.; Singleton, D. A. *J. Am. Chem. Soc.* **2005**, *127*, 9216. (g) Wang, Z. H.; Hirschi, J. S.; Singleton, D. A. *Angew. Chem., Int. Ed.* **2009**, *48*, 9156.

(29) Xu, L.; Doubleday, C. E.; Houk, K. N. *J. Am. Chem. Soc.* **2011**, *133*, 17848.

(30) (a) Xu, L.; Doubleday, C. E.; Houk, K. N. *Angew. Chem., Int. Ed.* **2009**, *48*, 2746. (b) Xu, L.; Doubleday, C. E.; Houk, K. N. *J. Am. Chem. Soc.* **2010**, *132*, 3029. (c) Huang, C.-H.; Tsai, L.-C.; Hu, W.-P. *J. Phys. Chem. A* **2001**, *105*, 9945. (d) Aktah, D.; Passerone, D.; Parrinello, M. *J. Phys. Chem. A* **2004**, *108*, 848. (e) Kelly, E.; Seth, M.; Ziegler, T. *J. Phys. Chem. A* **2004**, *108*, 2167. (f) Noguchi, N.; Nakano, H. *J. Chem. Phys.* **2009**, *130*, 154309. (g) Thomas, J. B.; Waas, J. R.; Harmata, M.; Singleton, D. A. *J. Am. Chem. Soc.* **2008**, *130*, 14544. (h) Wang, Z.; Hirschi, J. S.; Singleton, D. A. *Angew. Chem., Int. Ed.* **2009**, *48*, 9156. (i) Vayner, G.; Addepalli, S. V.; Song, K.; Hase, W. L. *J. Chem. Phys.* **2006**, *125*, 014317. (j) Black, K.; Liu, P.; Xu, L.; Doubleday, C.; Houk, K. N. *Proc. Natl. Acad. Sci. U. S. A.* **2012**, *109*, 12860.